12. J. Hwang, T. Timusk, G. D. Gu, *Nature* **427**, 714 (2004).
13. C. M. Varma, *Phys. Rev. B* **55**, 14554 (1997).
14. A. Lanzara *et al.*, *Nature* **412**, 510 (2001).
15. J. Lee *et al.*, *Nature* **442**, 546 (2006).
16. J. F. Zasadzinski *et al.*, *Phys. Rev. Lett.* **87**, 067005 (2001).
17. J. C. Campuzano, M. R. Norman, M. Randeria, in *The Physics of Superconductors*, K. H. Bennemann, J. B. Ketterson, Eds. (Springer-Verlag, Berlin, 2003), pp. 167–265.
18. T. Cuk *et al.*, *Phys. Status Solidi B* **242**, 11 (2005).
19. J. Fink *et al.*, in *Very High Resolution Photoelectron Spectroscopy*, S. Hüfner, Ed. (Springer, Berlin, 2007), pp. 295–325.
20. J. Hwang, E. J. Nicol, T. Timusk, A. Knigavko, J. P. Carbotte, *Phys. Rev. Lett.* **98**, 207002 (2007).
21. D. J. Scalapino, *Nat. Phys.* **2**, 593 (2006).
22. C. Howald, P. Fournier, A. Kapitulnik, *Phys. Rev. B* **64**, 100504 (2001).
23. S. H. Pan *et al.*, *Nature* **413**, 282 (2001).
24. K. K. Gomes *et al.*, *Nature* **447**, 569 (2007).
25. J. Bardeen, *Science* **181**, 1209 (1973).
26. W. L. McMillan, J. M. Rowell, *Phys. Rev. Lett.* **14**, 108 (1965).
27. D. J. Scalapino, J. R. Schrieffer, J. W. Wilkins, *Phys. Rev.* **148**, 263 (1966).
28. G. M. Eliashberg, *Sov. Phys. JETP* **11**, 696 (1960).
29. W. L. McMillan, J. M. Rowell, in *Superconductivity*, R. D. Parks, Ed. (Dekker, New York, 1969), pp. 561–613.
30. M. C. Boyer *et al.*, *Nat. Phys.* **3**, 802 (2007).
31. J. M. Valles, S.-Y. Hsu, R. C. Dynes, J. P. Garno, *Physica B (Amsterdam)* **197**, 522 (1994).
32. M. Le Tacon *et al.*, *Nat. Phys.* **2**, 537 (2006).
33. R. C. Dynes, V. Narayanamurti, J. P. Garno, *Phys. Rev. Lett.* **41**, 1509 (1978).
34. A. C. Fang *et al.*, *Phys. Rev. Lett.* **96**, 017007 (2006).
35. M. R. Norman, M. Randeria, H. Ding, J. C. Campuzano, *Phys. Rev. B* **57**, R11093 (1998).
36. S. Pilgram, T. M. Rice, M. Sigrist, *Phys. Rev. Lett.* **97**, 117003 (2006).
37. F. C. Niestemski *et al.*, *Nature* **450**, 1058 (2007).
38. M. Eschrig, M. R. Norman, *Phys. Rev. B* **67**, 144503 (2003).
39. R. C. Dynes, J. M. Rowell, *Phys. Rev. B* **11**, 1884 (1975).
40. K. E. Kihlstrom, T. H. Geballe, *Phys. Rev. B* **24**, 4101 (1981).
41. On changing the temperature, the sample drifts laterally relative to the tip. We obtain large data sets at each temperature that include a common field of view. The topographic features are then used to crop the area common to all temperatures to within 2 Å.
42. The tunneling conductance depends on a matrix element that may have energy dependence over several hundred millielectron volts. The spectral shapes of the normal state shown in Figs. 4 and 5 have been reproduced with several tips made from both Pt-Ir as well as W. The position of the hump can vary by up to 100 mV between tips.
43. D. van der Marel *et al.*, *Nature* **425**, 271 (2003).
44. W. Meevasana *et al.*, *Phys. Rev. B* **75**, 174506 (2007).
45. J. Graf *et al.*, *Phys. Rev. Lett.* **98**, 067004 (2007).
46. A. Damascelli, Z. Hussain, Z.-X. Shen, *Rev. Mod. Phys.* **75**, 473 (2003).
47. A. Paramekanti, M. Randeria, N. Trivedi, *Phys. Rev. Lett.* **87**, 217002 (2001).
48. P. W. Anderson, *Nat. Phys.* **2**, 626 (2006).
49. K. Haule, G. Kotliar, *Phys. Rev. B* **76**, 104509 (2007).
50. K. McElroy *et al.*, *Science* **309**, 1048 (2005).
51. E. Dagotto, *Science* **309**, 257 (2005).
52. Our studies were inspired by discussions with D. J. Scalapino and P. W. Anderson. We also thank R. Melko and D. J. Scalapino for help with the analysis of the low-energy electron-boson coupling. The work at Princeton is supported by the U.S. Department of Energy (DOE) under contract DE-FG02-07ER46419 and NSF through the Princeton Center for Complex Materials. Y.A. was supported by KAKENHI 19674002. The work in BNL is supported by DOE under contract DE-AC02-98CH10886.

Supporting Online Material

www.sciencemag.org/cgi/content/full/320/5873/196/DC1
SOM Text S1 and S2
Figs. S1 and S2
References

28 December 2007; accepted 27 February 2008
10.1126/science.1154700

Surface Mobility of Postsynaptic AMPARs Tunes Synaptic Transmission

Martin Heine,[1]* Laurent Groc,[1] Renato Frischknecht,[4] Jean-Claude Béïque,[3] Brahim Lounis,[2] Gavin Rumbaugh,[3] Richard L. Huganir,[3] Laurent Cognet,[2] Daniel Choquet[1]†

AMPA glutamate receptors (AMPARs) mediate fast excitatory synaptic transmission. Upon fast consecutive synaptic stimulation, transmission can be depressed. Recuperation from fast synaptic depression has been attributed solely to recovery of transmitter release and/or AMPAR desensitization. We show that AMPAR lateral diffusion, observed in both intact hippocampi and cultured neurons, allows fast exchange of desensitized receptors with naïve functional ones within or near the postsynaptic density. Recovery from depression in the tens of millisecond time range can be explained in part by this fast receptor exchange. Preventing AMPAR surface movements through cross-linking, endogenous clustering, or calcium rise all slow recovery from depression. Physiological regulation of postsynaptic receptor mobility affects the fidelity of synaptic transmission by shaping the frequency dependence of synaptic responses.

The fidelity of synaptic transmission between coupled neurons depends on their ability to transmit activity over a wide range of frequencies. Because of the relative slowness of chemical transmission, synaptic transmission acts as a low-pass filter with a cutoff between 10 and 100 Hz (*1*). When a presynaptic cell is stimulated at repetitive short intervals, the postsynaptic response usually decreases over time, the rate of depression being faster as the stimulus frequency increases (*2*). Most studies explain paired-pulse depression (PPD) as a combination of depression of presynaptic glutamate release and intrinsic kinetic properties of postsynaptic AMPARs upon agonist binding (*2*). Return from depression is believed to arise from recovery of release, together with AMPAR exit from desensitization. This assumes that AMPARs are stable within the postsynaptic density (PSD). Dynamic imaging has shown that AMPARs are not static but diffuse rapidly at the surface of neurons, traveling micrometer distances per second by random movements both in the synaptic and extrasynaptic membranes (*3*–*8*). Traffic of AMPARs from and to synapses through endo/exocytosis takes place in tens of minutes (*9*, *10*). However, lateral diffusion allows AMPARs to explore the synapse in the second range (*6*, *8*, *11*), which suggests that surface AMPAR trafficking might be implicated in faster processes.

Cross-linking of surface AMPARs decreases the coefficient of variation and increases PPD. We measured the variations in the efficacy of synaptic transmission in response to changes in AMPAR mobility by specific cross-linking (X-link) of GluR2-AMPARs with antibodies against their extracellular N-terminal domains (*4*, *11*) (fig. S1, A and B). Pairs of monosynaptically connected cultured hippocampal neurons were recorded using dual whole-cell recordings (Fig. 1A, fig. S1, C and D, and table S1) (*12*). Evoked excitatory postsynaptic currents (eEPSCs) were not affected by X-link (fig. S1, E to G). The coefficient of variation (CV) of eEPSCs over time and paired eEPSCs are classically used to measure synaptic transmission variability (*13*). Interestingly, the CV after X-link was lower than in control (control, 0.33 ± 0.02; X-link, 0.25 ± 0.02; *t* test, $P < 0.05$) (Fig. 1, B and C). Furthermore, paired-pulse eEPSCs at 50-ms intervals displayed PPD for the majority of the recorded neuron pairs (24 out of 31) (Fig. 1D). The remaining neuron pairs displayed paired-pulse facilitation. After X-link of GluR2, pairs displayed a more pronounced PPD, measured as a decrease in paired pulse ratio (PPR) (PPR in control, 0.86 ± 0.02; after X-link, 0.71 ± 0.04; *t* test, $P < 0.05$) (Fig. 1, D and E).

Variations in CV and PPR are usual hallmarks of presynaptic changes (*2*, *13*). GluR2 X-link should in contrast lead to changes in postsynaptic properties. Rapid AMPAR movements inside synapses (*6*–*8*) or between synaptic and extrasynaptic sites (*4*, *6*, *8*, *11*), could theoretically lead to variations in AMPARs' density at the postsynaptic side causing variability in eEPSCs, including in the rate of recovery from PPD, by regulating the exchange of desensitized receptors for naïve receptors.

AMPAR mobility inside synapses. To measure the fraction of surface receptors that are mobile in the extrasynaptic membrane or within a spine head both in CA1 pyramidal neurons from hippocampal slices and in cultured hippocampal neurons, we used fluorescence recovery after photobleaching (FRAP) on AMPAR sub-

[1]CNRS, UMR 5091, Université Bordeaux, Bordeaux, France. [2]Centre de Physique Moleculaire Optique et Hertzienne, CNRS, UMR 5798, Université Bordeaux, Talence, France. [3]Department of Neuroscience, Johns Hopkins University, Baltimore, MD, USA. [4]Leibniz Institut für Neurobiologie, Magdeburg, Germany.

*Present address: Leibniz Institut für Neurobiologie, Magdeburg, Germany.

†To whom correspondence should be addressed: dchoquet@u-bordeaux2.fr

units tagged at their N termini with super-ecliptic phluorin (*4*), a pH-sensitive form of green fluorescent protein (pHGFP) (Fig. 2, A to C, and fig. S2). GluR1::pHGFP was mostly homogenously distributed along the spines and dendrites, with occasional spines displaying strongly clustered GluR1::pHGFP. In contrast, GluR2::pHGFP was more systematically clustered within spine heads (fig. S2, A and B). A significant fluorescence recovery occurred in both shaft dendrite (~60% in 60 s) and spines (~30%) in hippocampal brain slices (Fig. 2, A to C), indicating that GluR2-AMPAR are mobile in intact hippocampi, as in cultured neurons (*5*, *7*–*9*). In cultures, GluR1::pHGFP and GluR2::pHGFP fluorescence also recovered after photobleaching, to a higher extent in extrasynaptic areas than in synaptic ones. About half of AMPARs exchanged from an extrasynaptic to a synaptic location for GluR2::pHGFP and nonclustered GluR1::pHGFP (Fig. 2C).

Individual GluR1- and GluR2-AMPARs were tracked using single quantum dots or organic dyes (*6*–*8*, *11*, *12*, *14*). Synapses were identified by Mitotracker (*7*, *8*) or the excitatory postsynaptic protein Homer1C::DsRed (*15*). In control, 70% of GluR1-AMPARs were mobile in the postsynaptic membrane, and half of this population exchanged continuously between synaptic and extrasynaptic domains, the other half being mobile but confined in the synapse (Fig. 2D and fig. S3) (*3*, *4*, *6*–*8*, *11*). The instantaneous diffusion coefficient, D, of mobile synaptic receptors ($D > 0.0075\ \mu m^2/s$) was comparable for quantum dot (QD) or single dye (SD)–labeled receptors (Fig. 2E). These exchanging AMPARs only dwell for a few seconds in the synapse (Fig. 2G and fig. S3); the remaining AMPARs were transiently immobile. As expected, antibody-induced AMPARs X-link massively reduced receptor mobility and suppressed the exchange of receptors between synaptic and extrasynaptic sites (fig. S1, A and B).

AMPAR mobility contributes to recovery from PPD. Because PPD has been mainly envisioned as influenced by presynaptic processes (*2*, *13*), we investigated the effect of receptor immobilization on isolated postsynaptic AMPAR-mediated currents. For this, glutamate-evoked currents were recorded in whole-cell mode using rapid iontophoretic glutamate application onto synapses (identified by Homer1C::DsRed) (figs. S4 and S5). In control, application of glutamate for 1 ms with iontophoretic currents of ~100 to 200 nA evoked inward currents of 130.4 ± 11 pA (n = 37) with fast rise and decay times (Fig. 3A and fig. S5). When paired glutamate applications were applied, the second response was depressed (Fig. 3 and fig. S5). The extent of depression decreased as the time interval between paired glutamate applications increased, as expected from AMPARs' recovery from desensitization (*16*–*19*). Indeed, PPD was abolished by cyclothiazide (50 μM) (Fig. 3, A and B, and fig. S6A), an antagonist of AMPAR desensitization (*20*, *21*).

However, AMPAR immobilization through X-link reduced the response amplitude to the second contiguous glutamate application (Fig. 3, A and B). The X-link–induced reduction in paired-pulse ratio was dependent on the interstimulus interval, with a maximal effect (factor 2) for short intervals (10 to 20 ms) and no effect over 200 ms. Receptor X-link thus modified the characteristic time and the extent of recovery from depression.

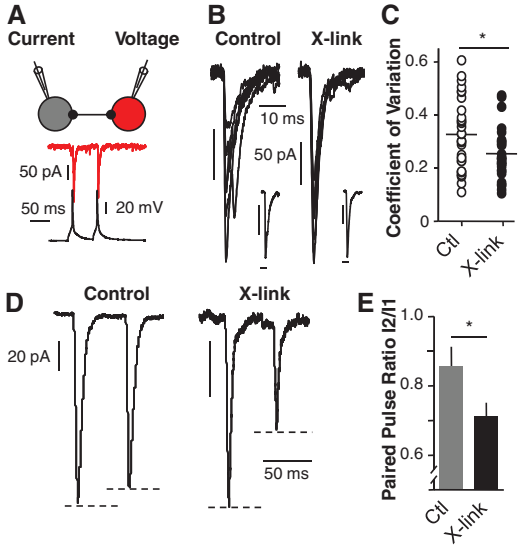

Fig. 1. AMPAR immobilization increases PPD and decreases variability. (**A**) Sample whole-cell recordings of a connected pair of cultured hippocampal neurons. The presynaptic neuron was recorded in current-clamp at 0 pA and the postsynaptic neuron voltage-clamped at −60 mV. A pair of depolarizing pulses in the presynaptic cell separated by 50 ms triggered action potentials that each elicited an AMPAR-mediated EPSC in the postsynaptic neuron. (**B**) Series of evoked EPSCs elicited at 10-s intervals in control conditions or at least 10 min after X-link surface GluR2-containing AMPARs with an antibody to GluR2 followed by a secondary antibody to immunoglobulin G (IgG). (**C**) Plot of the coefficient of variation of EPSCs recorded as in (B) in 24 cells. GluR2 X-link decreases variability. $P < 0.05$. (**D** and **E**) Paired-pulse traces of EPSCs recorded as in (A) in control conditions or at least 10 min after X-link surface GluR2. These are different cells from the same culture batch.

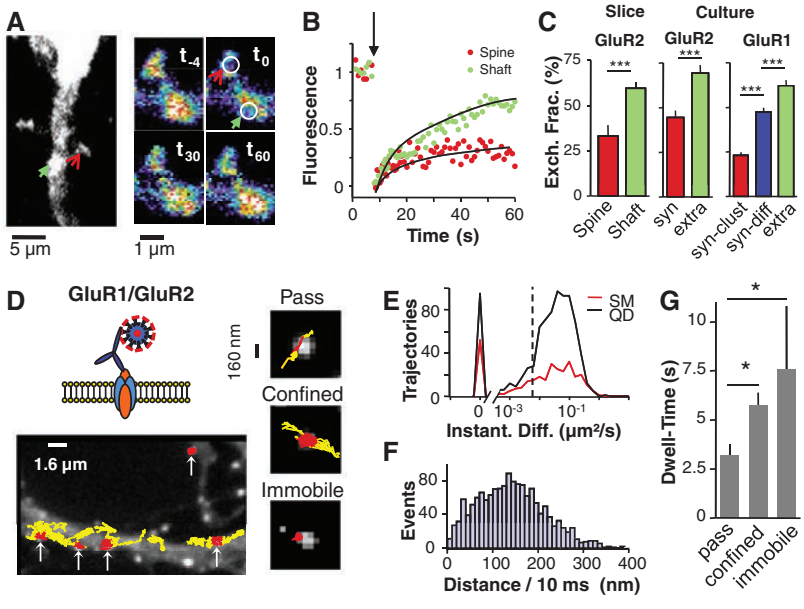

Fig. 2. Mobility of AMPARs in synapses form brain slices and cultured neurons. (**A**) Imaging of GluR2::pHGFP in live CA pyramidal neurons from hippocampal slices. Fluorescence was photobleached (t_0) in spine (circles, red open arrow) and dendritic shaft (circles, green filled arrow). (**B**) Fluorescence recovery versus time in the photobleached areas in (A). (**C**) Averaged recovered fraction of GluR2::pHGFP in dendritic shaft (n = 41) or spine (n = 19) in hippocampal slices and 21 days in vitro (DIV) cultured hippocampal neurons expressing GluR2::pHGFP (n = 28) or GluR1::pHGFP (n = 40). (**D**) Trajectories of GluR1-containing AMPARs on dendrites of a 21-DIV cultured Homer1C::DsRed transfected hippocampal neuron. (Top) Diagram of AMPARs labeling with a QD through GluR1 antibody. (Bottom left) Imaged dendritic segment. Postsynaptic sites accumulate DsRed (arrows). Extrasynaptic (yellow) and synaptic (red) trajectories of QD-labeled GluR1 receptors recorded for 66 s are plotted. (Right) Trajectories on Homer1C::DsRed labeled postsynaptic sites for the three categories of observed diffusion behaviors within the synapse. (**E**) Histogram distribution of the instantaneous diffusion coefficients of synaptic trajectories obtained from GluR1-coupled QDs or Cy3 single dye molecule (SM). Dotted line is the threshold below which receptors are counted as immobile. (**F**) Frequency distribution of the displacement (Δt = 10 ms) of mobile GluR1 receptors within the synapse (median = 0.14 nm ± interquartile range (IQR) 0.08/0.19 nm). (**G**) Histogram of the mean ± SEM dwell time of GluR1 receptors in synapses, sorted by their diffusion properties (n = 10). For immobile receptors, only those transiently stabilized in the synapse are counted. $P < 0.05$.

PPD was absent at extrasynaptic sites (PPR = 1.12 ± 0.15; n = 4), where AMPARs are more mobile and not confined (fig. S3) (*4*, *7*, *8*). Activation of successive AMPAR currents by two-photon 4-methoxy-7-nitroindolinyl-caged L-glutamate (MNI-glutamate) uncaging (2P-EPSCs) (*22*) provided comparable sensitivity to X-link, although a significant PPD was already present in control conditions at synaptic and extrasynaptic sites (Fig. 3, C and D, and fig. S7). In control, PPR was significantly higher after uncaging onto shaft regions compared with uncaging at the tip of closely located spines, where receptors are less mobile (Fig. 2). After GluR1 X-link, PPR onto shafts was decreased compared with controls and was no longer different than that onto spines (Fig. 3, C and D).

Several controls were performed to refute the possibility that antibody X-link modified the amount of recovery from depression through changes of receptor desensitization. First, primary antibody binding to the receptors did not modify the basic properties of mEPSCs (fig. S8, A and B). Second, X-link of the receptors did not modify individual glutamate-evoked iontophoretic responses (fig. S8, C to G). Third, the application of cyclothiazide totally abolished the decrease in recovery rate between glutamate applications induced by receptor X-link (Fig. 3, A and B, and fig. S7). Fourth, the kinetic properties of AMPARs were identical with and without antibodies, as measured in excised outside-out recordings (fig. S9).

The recovery from depression did not depend on receptor mobility during glutamate application to large membrane areas [iontophoretic current > 300 nA/1 ms (Fig. 3E); activated area ~2.5 μm (fig. S5C)]. At low iontophoretic currents (I < 100 nA/1 ms), receptors were activated over a small area (<0.5 μm) (Fig. 3E and fig. S5C), and PPD was only present after receptor immobilization. The parallel decrease in PPR and increase in iontophoretic current likely reflect prolonged presence of glutamate to desensitize receptors (*18*, *23*, *24*). That receptor immobilization only modifies PPR at low iontophoretic current amplitudes suggests that recovery from depression due to receptor movements in a large glutamate application zone is slower than the rate of recovery from desensitization of individual receptors.

To investigate this, we used the rapidly dissociating glutamate receptor antagonist kynurenic acid (Kyn) to modify the apparent spatiotemporal glutamate waveform. Kyn generates a block that is inversely related to glutamate concentration (*25*). Kyn (1 mM) reduced the current amplitude and accelerated the decay of iontophoretically elicited AMPAR currents (Fig. 3G) (*25*). The presence of Kyn reduced PPD in control but not in X-linked conditions (Fig. 3F). In the presence of Kyn, the area where AMPARs are activated and/or desensitized is smaller, allowing for their faster exchange with naïve AMPARs during the interpulse interval.

Interplay between AMPAR diffusion and recovery from PPD. To study the respective contributions of AMPAR recovery from desensitization and AMPAR mobility to the recovery from PPD, we took advantage of the fact that pHGFP::GluR1 can be either clustered or diffuse at synaptic sites, with slower mobility when clustered (Fig. 2C and fig. S2). Overexpression of the GluR1 subunit increases the formation of GluR1 homomeric receptors (*26*), which desensitize faster than heteromeric receptors but recover from desensitization one-third as fast (*27*). Thus, the rate of recovery from PPD should reflect the prolonged exit of receptors from a desensitized state mainly when lateral diffusion rate is low.

PPD was similar at synaptic sites of nontransfected neurons and at synapses expressing diffuse pHGFP::GluR1 in transfected neurons. In contrast, synapses with clustered pHGFP::GluR1 displayed a much stronger PPD (Fig. 4, A to C). Thus, recovery from PPD is dominated by receptor diffusion when pHGFP::GluR1 is highly mobile, whereas it is dominated by the intrinsic kinetic properties of GluR1 when pHGFP::GluR1 has a low mobility. We therefore specifically immobilized pHGFP::GluR1 containing receptors by X-link with an antibody to GFP (Fig. 4, A to C). PPD was strong in areas of clustered receptors, approaching the value obtained for not X-linked but clustered pHGFP::GluR1 receptors. PPD was more pronounced for immobilized GluR1

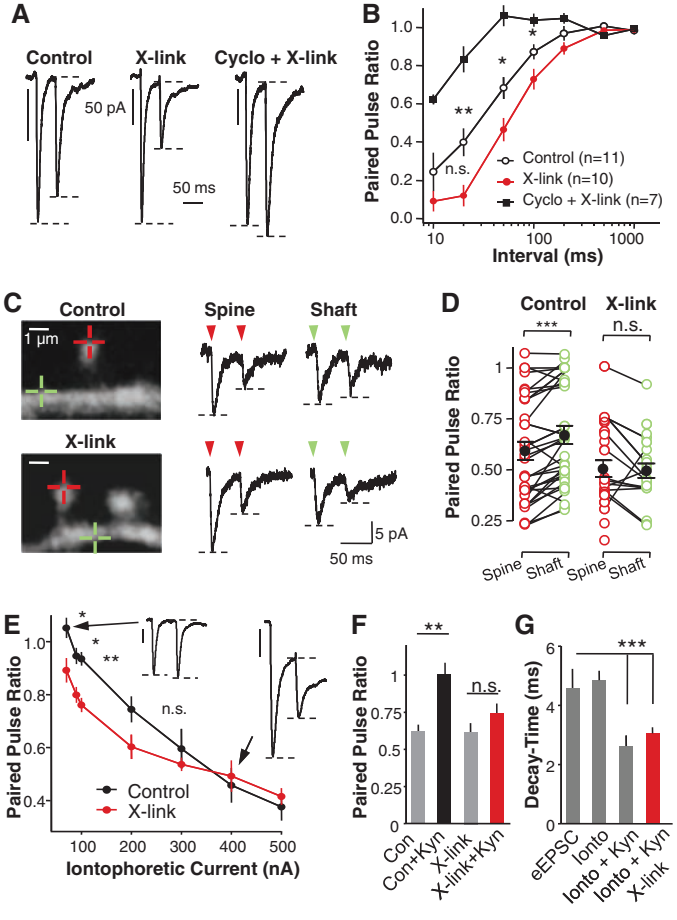

Fig. 3. AMPAR immobilization impedes recovery from depression during paired-pulse application of glutamate. (**A**) Whole-cell recordings of currents elicited by paired iontophoretic applications of glutamate to synaptic sites in control neurons (left), after X-link surface GluR2-containing AMPARs without (middle) or with (right) 50 μM cyclothiazide. Pulse interval is 50 ms; traces are averaged from 10 recordings. (**B**) Plot of the recovery rate as a function of interpulse interval; control (n = 11), X-link GluR2 (n = 15), with 50 μM cyclothiazide (n = 10). (**C**) (Left) Confocal images of individual spines and surrounding shaft area used to induce successive (50 ms apart) 2P-EPSCs in control (top) or after X-link of GluR1 (bottom). Uncaging spots were positioned (crosses) either at the spine tip (red) or on shaft (green). (Right) Current traces, uncaging at arrows. (**D**) Scattered plots of PPRs of 2P-EPSCs induced at spines or shaft regions in control conditions (n = 33 spines and shafts) and after X-link of GluR1 (n = 28 spines; shaft n = 22). Mean ± SEM is indicated by the black dots, and pairs of closely positioned spines and shafts are indicated by the connected lines (***P < 0.01). (**E**) Plot of the PPR versus applied iontophoretic current amplitude; control (n = 13), X-link (n = 8). (Insets) Sample traces for paired iontophoretic glutamate application (left, 90 nA/1 ms; right, 400 nA/1 ms). Scale bar, 50 pA (left), 100 pA (right). (**F**) Mean ± SEM of PPR for paired iontophoretic glutamate application (200 nA/1 ms) in control or after X-link of GluR2, without (Con) or with 1 mM kynurenic acid (Kyn) under the indicated conditions. n = 5 for each condition. (**G**) Mean ± SEM decay time constant of EPSCs, of currents evoked by iontophoretic glutamate application (200 nA/1 ms) in control (ionto), with 1 mM kynurenic acid (Kyn) before or after X-link of GluR2 (kyn + X-link).

containing clusters than immobilized wild-type AMPARs that recover faster from desensitization (*27*). The rectification index showed that the relative proportion of homomeric GluR1 receptors at synapses did not correlate with the clustered state of GluR1 and was unchanged by X-link (Fig. 4, D and E).

Calcium-induced AMPAR immobilization increases PPD. Because spontaneous clustering of AMPARs modified the extent of PPD, physiological processes that regulate AMPARs' mobility might also regulate PPD. AMPAR mobility is strongly decreased by local rises in intracellular calcium (*5*). We explored whether an increase in calcium triggered by physiological synaptic stimulations also modifies PPD. Stimulation of a large population of synapses at 50 Hz, but not 5 Hz, induced a profound decrease in AMPARs' mobility (Fig. 5A). This immobilization was stronger for GluR1 than GluR2 (explored surface, percentage of control, GluR2 83.1 ± 4%, GluR1 50 ± 5%, 5 min after stimulation). Stimulations of 50 Hz induced a stronger immobilization at synaptic than at extrasynaptic sites, accompanied by a reduction in the percentage of receptors that exchange between synaptic and extrasynaptic sites (Fig. 5, B to D). This immobilization was due to rises in intracellular calcium through activation of calcium-permeable *N*-methyl-D-aspartic acid receptors (NMDARs) (Fig. 5D and fig. S10) and did not alter the proportion of endocytosed GluR1-containing AMPARs (control 15 min, 12.5 ± 3%; 15 min after 50 Hz, 11.6 ± 4%). Diffusion of another membrane receptor N-Cam did not change after stimulation (Fig. 5, B and C). Immobilization of AMPARs was accompanied by an increase in PPD at a subpopulation of synapses after 50-Hz stimulation (Fig. 5, E and F), indicating that physiological immobilization of AMPARs also has an impact on recovery from synaptic depression.

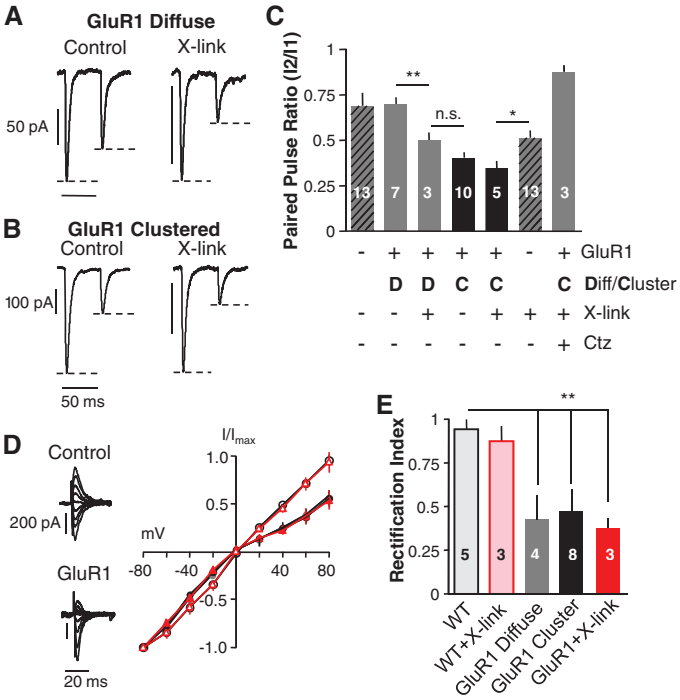

Fig. 4. Endogenous clustering of AMPARs increases PPD. (**A** and **B**) Sample whole-cell recordings of currents elicited by paired iontophoretic applications of glutamate to synaptic sites displaying diffuse (A) or clustered (B) GluR1 distribution in control neurons (left) or after X-link surface pHGFP::GluR1 by antibody to GFP (right). (**C**) Histograms of mean PPR ± SEM in the conditions exemplified in (A) and (B) and in controls. Measurements from recordings at Homer::DsRed synaptic sites in neurons expressing (GluR1+) or not (GluR1–) pHGFP::GluR1, with or without antibody to GFP–mediated X-link. Synaptic sites were sorted as bearing either a diffuse (D) or clustered (C) pHGFP::GluR1 distribution. One series of experiments is in the presence of cyclothiazide (Ctz). (**D**) (Left) Whole-cell currents elicited by iontophoretic applications of glutamate to synaptic sites recorded at various holding potentials in nontransfected (control) and pHGFP::GluR1 (GluR1)–expressing neurons. (Right) Plots of mean *I-V* curves for currents in the left. The curve is linear for control cells (empty circles), whereas it rectifies in pHGFP::GluR1-expressing neurons, at similar levels whether clustered (filled black circles) or diffuse (filled gray circles), indicating the higher proportion of GluR1 homomeric AMPARs. X-link either endogenous receptors with an antibody to GluR2 (empty triangles) or pHGFP::GluR1 with an antibody to GFP (filled triangles) does not modify the rectification index as compared to its matched control. (**E**) Mean + SEM of the rectification index in the indicated conditions.

Discussion. We report that AMPAR lateral diffusion influences synaptic transmission at different time scales. On the second to minutes time scale, the CV of synaptic currents depends in part on the surface trafficking of AMPARs that diffuse within the PSD and exchange between synaptic and extrasynaptic sites. In the tens of millisecond time scale, AMPAR lateral diffusion regulates the fast recovery from postsynaptic depression induced at high-frequency transmitter release. Consequently, we now propose that the rate of recuperation from synaptic depression results from the combination of the recovery of AMPAR from desensitization, the recuperation of transmitter release (*2*), and the fast lateral exchanges of desensitized receptors with naïve functional ones. In addition, the rate of AMPAR fluxes can be modulated in various physiological ways, such as clustering states or variations in intracellular calcium, and these regulations affect the synaptic signaling.

The role of AMPARs' desensitization during PPD at hippocampal synapses is debated (*18*, *28*–*31*), in part due to the absence of adequate tools (e.g., cyclothiazide having both presynaptic and postsynaptic effects) (*32*, *33*). The desensitization properties of AMPARs will depend on the glutamate clearance, particularly at synapses whose morphologies favor spillover from neighboring release sites (*19*, *34*–*39*). Measurements of AMPAR-mediated current amplitude and kinetics, as well as theoretical calculations, have suggested that the size of the field where receptors are occupied by glutamate only represents a subarea of the PSD that spans about 100 nm from the site of vesicle release and is only about 25% of the area of an average CA1 synapse for a single quantal release (*13*, *36*, *40*, *41*). At least 50% of the AMPARs are mobile at synaptic sites and can explore the whole PSD (*4*, *7*, *8*). Our single-molecule measurements, which likely underestimate receptor mobility (*42*), indicate that AMPARs can diffuse at rates above 0.25 $\mu m^2/s$ and can thus move >100 nm in 10 ms. This is sufficient to escape the area reached by glutamate within a short time (*13*). Within a region of 200-nm diameter, calculations indicate that ~30% of receptors are replaced within 10 ms by diffusion at 0.1 $\mu m^2/s$ (figs. S11 and S12C). Thus, the replacement of desensitized receptors occurs at a characteristic time (50% in 30 ms if all receptors are mobile at 0.1 $\mu m^2/s$ and escape from a 200-nm zone) similar to, or even faster than, that of the recovery of individual AMPAR from desensitization (50% in 40 to 60 ms). Along this line, PPR was more pronounced with uncaging than with iontophoresis, even at low amplitudes of AMPAR-mediated currents, likely due to the larger size of the uncaging spot versus the iontophoretic one.

The extent of frequency-induced synaptic depression depends on desensitization, glutamate release, and postsynaptic receptor redistribution rate. This notion is supported by a theoretical model that combines previously established parameters of glutamate release in the synaptic cleft, AMPAR activation, and desensitization kinetics schemes (*13*, *39*, *43*) with receptor mobility (fig. S11). The theoretical recovery of AMPAR currents from depression strongly depends on lateral diffusion, on the area over which receptors are activated, and on receptor confinement (fig. S12).

Postsynaptic receptors' mobility is acutely regulated by physiological processes such as temperature (*8*), depolarization (*7*), glutamate (*8*), and tetanic stimulations leading to calcium-induced immobilization of receptors (this study). These changes in the fraction of mobile receptors will affect frequency-dependent depression in parallel to presynaptic processes (*13*). This could be involved in providing a postsynaptic mechanism to modify the frequency dependence

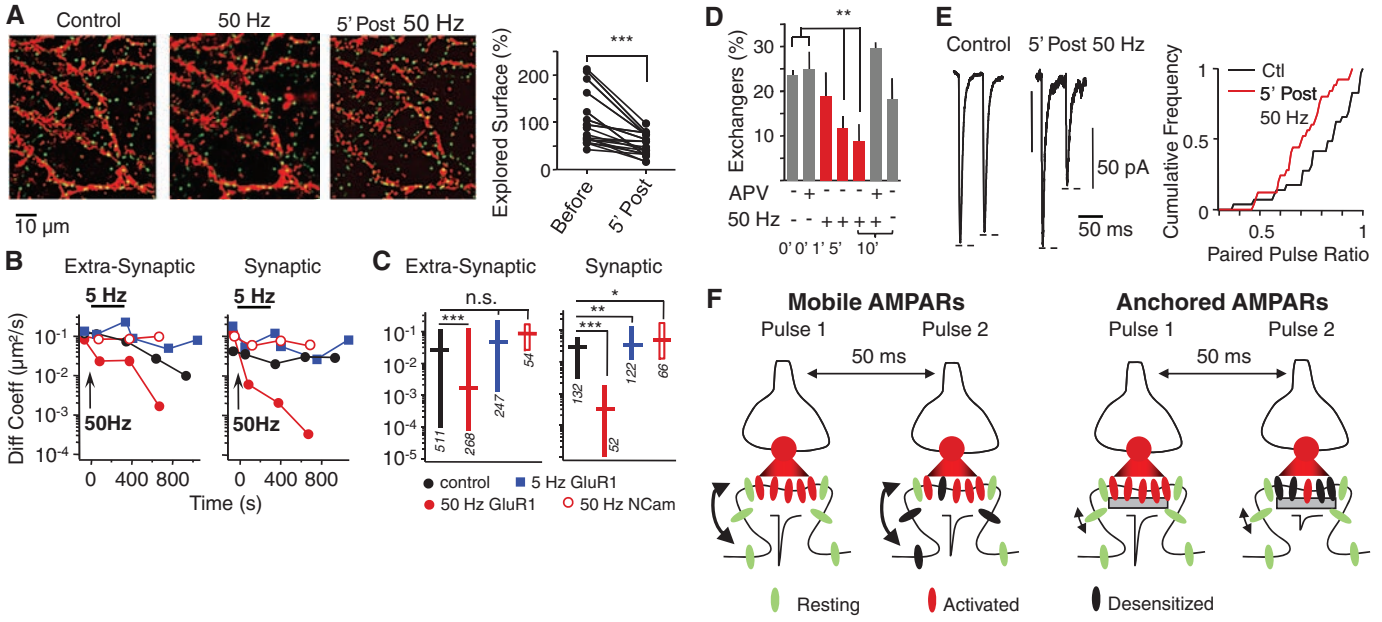

Fig. 5. Activity-dependent increase in intracellular calcium immobilize AMPARs and increase PPD. (**A**) (Left) Images of the cumulative surface explored (red) on dendrites by QDs bound to GluR1-containing AMPARs within 1 min of observation before, during, and 5 min after 50-Hz field stimulation (synapses in green). (Right) Summary plot of the evolution of the explored surface between the control recording period and 5 min after stimulation (n = 16). (**B** and **C**) Plots of the median of instantaneous diffusion coefficient versus time (B) or at 800 s (median ± IQR) of recording (C) for extrasynaptic (left) and synaptic (right) receptors. Both outside and inside synapses, stimulation at 5 Hz (blue squares) slightly increased receptor diffusion in comparison to the independent control (black circles), whereas 50-Hz stimulation (red circles) strongly decreased receptor mobility. Diffusion coefficient of N-cam (open red circles) was not changed after 50 Hz stimulation. (**D**) Plots of the mean fraction of GluR1 receptors that exchange between synaptic and extrasynaptic sites, with or without (2R)-amino-5-phosphonovaleric acid (APV), and before or at the indicated times after 50-Hz stimulation (n = 13). (**E**) (Left) Sample whole-cell currents elicited by paired iontophoretic applications of glutamate to synaptic sites before (top) and 5 min after (bottom) 50-Hz stimulation in different cells from the same culture. (Right) Cumulative frequency plot of the paired-pulse ratio recorded before (black line, 13 cells) and after (red line, 13 cells) 50-Hz stimulation. $P < 0.01$, Kolmogorov-Smirnov test. (**F**) Schematic diagram of the involvement of mobile AMPARs in regulating PPD. When AMPARs are largely mobile (left), AMPARs activated (red) and then desensitized (black) by a first glutamate release are rapidly exchanged by functional ones (green), which are then available for activation by a sequential glutamate release. In contrast, when AMPARs are immobilized (right), desensitized receptors remain in place, decreasing the amount of functional receptors available for activation by a sequential pulse.

of synaptic transmission after activity-dependent processes that trigger both short- and long-term synaptic plasticity.

References and Notes

1. E. S. Fortune, G. J. Rose, *Trends Neurosci.* **24**, 381 (2001).
2. R. S. Zucker, W. G. Regehr, *Annu. Rev. Physiol.* **64**, 355 (2002).
3. H. Adesnik, R. A. Nicoll, P. M. England, *Neuron* **48**, 977 (2005).
4. M. C. Ashby, S. R. Maier, A. Nishimune, J. M. Henley, *J. Neurosci.* **26**, 7046 (2006).
5. A. J. Borgdorff, D. Choquet, *Nature* **417**, 649 (2002).
6. M. D. Ehlers, M. Heine, L. Groc, M. C. Lee, D. Choquet, *Neuron* **54**, 447 (2007).
7. L. Groc *et al.*, *Nat. Neurosci.* **7**, 695 (2004).
8. C. Tardin, L. Cognet, C. Bats, B. Lounis, D. Choquet, *EMBO J.* **22**, 4656 (2003).
9. M. D. Ehlers, *Neuron* **28**, 511 (2000).
10. M. Passafaro, V. Piech, M. Sheng, *Nat. Neurosci.* **4**, 917 (2001).
11. C. Bats, L. Groc, D. Choquet, *Neuron* **53**, 719 (2007).
12. Materials and methods are available as supporting material on *Science* Online.
13. J. E. Lisman, S. Raghavachari, R. W. Tsien, *Nat. Rev. Neurosci.* **8**, 597 (2007).
14. M. Dahan *et al.*, *Science* **302**, 442 (2003).
15. Y. Sugiyama, I. Kawabata, K. Sobue, S. Okabe, *Nat. Methods* **2**, 677 (2005).
16. T. Otis, S. Zhang, L. O. Trussell, *J. Neurosci.* **16**, 7496 (1996).
17. K. M. Partin, M. W. Fleck, M. L. Mayer, *J. Neurosci.* **16**, 6634 (1996).
18. D. Colquhoun, P. Jonas, B. Sakmann, *J. Physiol.* **458**, 261 (1992).
19. I. M. Raman, L. O. Trussell, *Biophys. J.* **68**, 137 (1995).
20. L. O. Trussell, S. Zhang, I. M. Raman, *Neuron* **10**, 1185 (1993).
21. K. A. Yamada, C. M. Tang, *J. Neurosci.* **13**, 3904 (1993).
22. J. Béïque *et al.*, *Proc. Natl. Acad. Sci. U.S.A.* **103**, 19535 (2006).
23. B. K. Andrasfalvy, J. C. Magee, *J. Neurosci.* **21**, 9151 (2001).
24. M. A. Smith, G. C. Ellis-Davies, J. C. Magee, *J. Physiol.* **548**, 245 (2003).
25. J. S. Diamond, C. E. Jahr, *J. Neurosci.* **17**, 4672 (1997).
26. S. H. Shi *et al.*, *Science* **284**, 1811 (1999).
27. J. Grosskreutz *et al.*, *Eur. J. Neurosci.* **17**, 1173 (2003).
28. L. E. Dobrunz, C. F. Stevens, *Neuron* **18**, 995 (1997).
29. A. Arai, G. Lynch, *Brain Res.* **799**, 235 (1998).
30. G. O. Hjelmstad, J. T. Isaac, R. A. Nicoll, R. C. Malenka, *J. Neurophysiol.* **81**, 3096 (1999).
31. E. Hanse, B. Gustafsson, *J. Physiol.* **531**, 467 (2001).
32. T. Ishikawa, T. Takahashi, *J. Physiol.* **533**, 423 (2001).
33. J. S. Diamond, C. E. Jahr, *Neuron* **15**, 1097 (1995).
34. T. S. Otis, Y. C. Wu, L. O. Trussell, *J. Neurosci.* **16**, 1634 (1996).
35. M. A. Xu-Friedman, W. G. Regehr, *J. Neurosci.* **23**, 2182 (2003).
36. X. Xie, J. S. Liaw, M. Baudry, T. W. Berger, *Proc. Natl. Acad. Sci. U.S.A.* **94**, 6983 (1997).
37. M. V. Jones, G. L. Westbrook, *Trends Neurosci.* **19**, 96 (1996).
38. V. Scheuss, R. Schneggenburger, E. Neher, *J. Neurosci.* **22**, 728 (2002).
39. K. M. Franks, T. M. Bartol Jr., T. J. Sejnowski, *Biophys. J.* **83**, 2333 (2002).
40. K. M. Franks, C. F. Stevens, T. J. Sejnowski, *J. Neurosci.* **23**, 3186 (2003).
41. G. Liu, S. Choi, R. W. Tsien, *Neuron* **22**, 395 (1999).
42. L. Groc *et al.*, *J. Neurosci.* **27**, 12433 (2007).
43. P. Jonas, G. Major, B. Sakmann, *J. Physiol.* **472**, 615 (1993).

44. We thank E. Hanse, M. Ehlers, E. Gundelfinger, and A. Triller for helpful discussions; D. Perrais for outside-out experiments; C. Tigaret for producing the Sinbis pHGFP::GluR2 viral particles; C. Breillat, B. Tessier, and D. Bouchet for molecular biology and cell cultures; E. Normand for organotypic slice preparation; and E. Petrini for some control experiments. This work was supported by the Centre National de la Recherche Scientifique, the Conseil Régional d'Aquitaine, the Ministère de la Recherche, the Fondation pour la Recherche Médicale, the Human Frontier Science Program, the Association Française contre les Myopathies, European Community Grant CT-2005-005320, Howard Hughes Medical Institute (to R.L.H.), National Institute of Neurological Disorders and Stroke (to R.L.H.), the National Alliance for Research on Schizophrenia and Depression (to J.-C.B.), and postdoctoral fellowship HE-3604/1-1 for M.H. R.F. was supported by Deutsche Forschungsgemeinschaft project GU 230/5-2.

Supporting Online Material

www.sciencemag.org/cgi/content/full/320/5873/201/DC1
Materials and Methods
Figs. S1 to S12
Table S1
References

23 October 2007; accepted 15 February 2008
10.1126/science.1152089